Finite Element Analysis of Residual Stresses and Deformations in Direct Metal SLS Process

Wei Jiang
School of Mechanical Engineering, Dalian University of Technology, 116024, P.R. China

K.W. Dalgarno and T.H.C. Childs
School of Mechanical Engineering, University of Leeds, Leeds, LS2 9JT, U.K.

Abstract

Direct metal SLS processes use a high power laser beam to selectively fuse fully metallic powder to directly produce functional metal components or tooling. As a thermal dynamic process, it inevitably causes thermal stresses, stress-induced deformations and cracking. Understanding these is very important in controlling residual stresses and stress-induced deformations.

In this research, the residual stresses and deformations in direct laser sintering of stainless steel is investigated by an integrated thermal and mechanical model. Temperature-dependent material properties are taken into account in both models. Using a commercial finite element software, with sintered geometry and temperatures imported from a thermal model, the residual stresses and deformations of direct SLS of stainless steel are predicted. In the long term this will make it possible to achieve minimum residual stresses and deformations by controlling the SLS process parameters, material properties and other relevant parameters.

1. INTRODUCTION

Direct metal SLS processes use a high power laser beam to selectively fuse fully metallic powder to directly produce functional metal components or tooling [1,2]. It has the capability of reducing cycle time in product development, lowering cost, and building a very complex geometries. However, as a thermal dynamic process, SLS process inevitably causes thermal stresses, stress-induced deformations and cracking. Understanding these is very important in controlling residual stresses and stress-induced deformations and in developing SLS into industrial grade rapid manufacturing method.

Direct metal SLS processes are very complicated. During the process, metal powders under the laser beam undergo a phase change from solid to liquid and then back to solid within a very short time. This phase change is associated with latent heat, which has a significant effect on the temperature and residual stress distribution. Also the elevated temperature gradients present in this area both during the heating and the cooling, along with the sharp decrease in mechanical

properties during heating, yield non-homogeneous permanent strains and residual stresses after processing. Residual stress has a great influence on structural strength, loss of edge tolerance and inter-layer debonding.

Modeling direct metal SLS is a very challenging task. Although some SLS modelling work have been reported [3-7], it has concentrated on amorphous polymers. A thorough survey of the existing literature indicates that scant attention has been paid to the numerical modeling of direct metal laser sintering process. This paper reports finite element modeling of direct metal SLS. The residual stresses and deformations in direct metal laser sintering are investigated by an integrated thermal and mechanical model. In the thermal model, the nonlinear heat conduction equation with a moving Gaussian heat source is applied, and latent heat due to phase change is considered. The temperature-dependent material properties are taken into account in both models. By using ABAQUS commercial finite element software, with fully sintered geometries and temperatures imported from thermal model, the residual stresses and deformations in the direct SLS of 316 stainless steel are predicted. The objective of this work is to understand residual stresses build-up and to develop a process simulation to optimize the SLS process and to control it intelligently.

2. MODELLING

2.1 Method

The strategy to solve problems of thermally induced residual stress is to link heat transfer analysis to stress analysis, by an integrated thermal-mechanical model. Fig. 1 presents the analysis procedures.

In the thermal model, the governing principle of SLS process is modeled as non-linear heat conduction equation with a moving Gaussian heat source [8]. During direct metal SLS process, the powders undergo a phase change from solid to liquid and then back to solid. This phase change is associated with latent heat, and the temperature recovery method [9] is employed to take account of this. Temperature dependent thermal conductivity and specific heat are considered in the thermal model. In order to predict the density field and sintered geometry, the resulting temperature/time history is linked to a liquid-phase sintering law and mass conservation principle [10]. The shrinkage due to solidification is assumed only in the z direction, as shown in Fig. 2(a).

The transient temperatures, sintered geometry and density field are output from the thermal model. After filtering out unnecessary information by interface programs, the temperatures below the melting point and geometries of the fully sintered region are used as input to the mechanical model to predict the evolution of residual stresses and deformations. The temperature dependent elastic modulus and coefficient of thermal expansion are also considered in the mechanical model. This uncoupled approach assumes that deformations cause negligible temperature changes.

2.2 Geometry and Meshes

The finite element meshes used to discretize the geometry for the thermal and mechanical model are shown in Fig. 2.

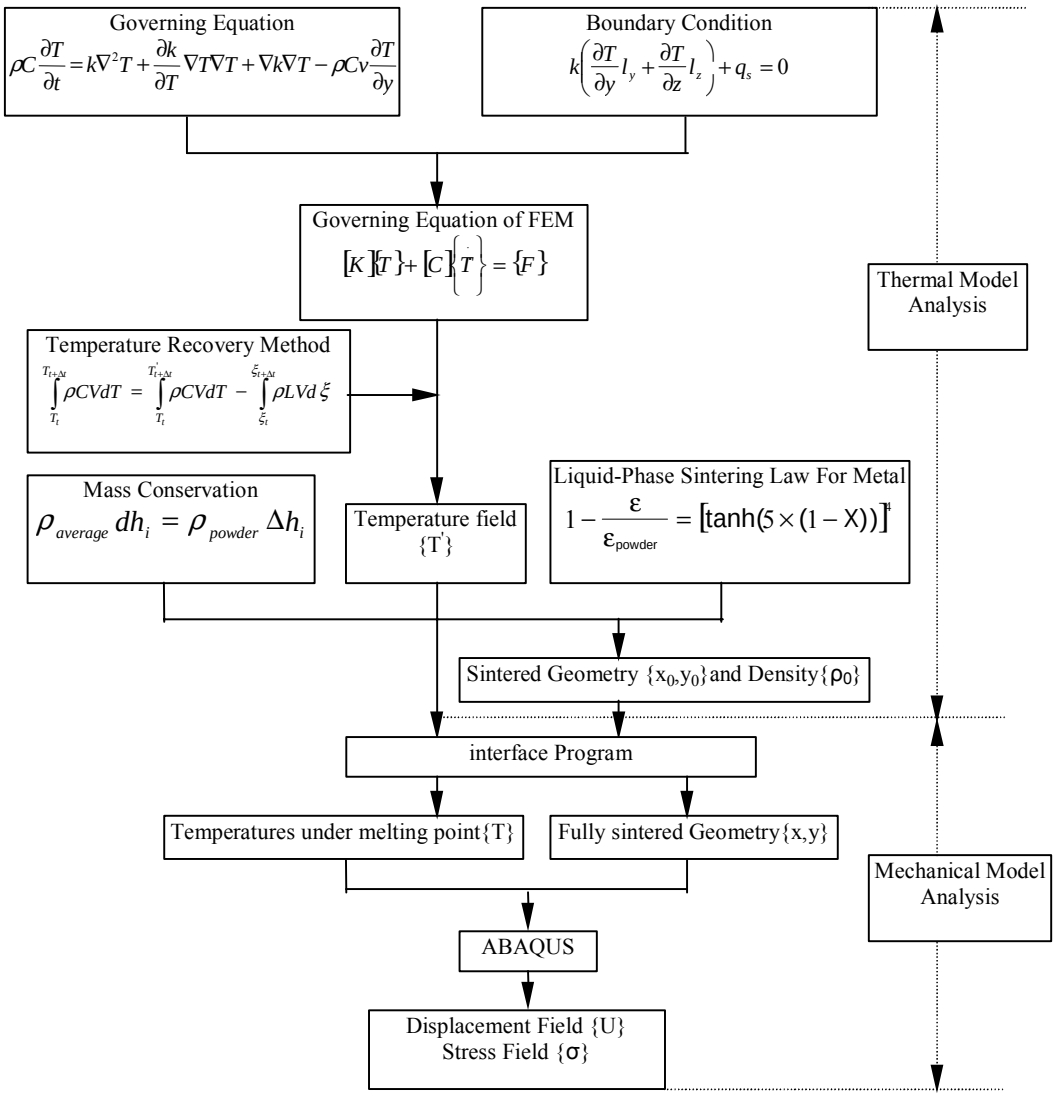

Figure 1 - Analysis Procedures, Notation From Table 1

Two kinds of meshes are used in the thermal model, thermal mesh and powder bed mesh. The thermal meshes are discretized into four-node brick elements, as shown in Fig. 2(a). Each four-node brick is regarded as a pair of three-node triangles. In order to accurately predict the large gradients of temperature near the heat source, the thermal mesh is relatively fine in the neighborhood of laser beam q_{laser}, its y-spacing is 1/6 of the beam diameter d (0.183 mm), and its z-spacing is 1/6 of the powder layer thickness $t_{layer,}$ (0.083 mm). The mesh coarsens with distance from the heat source in multiples of this fine mesh size. The powder bed mesh is of the same size as the fine thermal mesh. Linear interpolations are used to map between the powder bed meshes and

the thermal meshes. The thermal meshes superimpose on the powder bed, moving at v in the Y direction by d/6 in each time step.

Since partially sintered regions will not support thermal stresses, they were filtered out by an interface program. The geometries of the fully sintered region whose density is greater than 7800 kg/m^3 were imported to the mechanical model. The meshes in the mechanical model are of the same size as in the thermal model, that is 1/6 of laser beam diameter d in x-spacing and 1/6 of the powder layer thickness t_{layer} in y-spacing, as shown in Fig. 2(b). The fully sintered part is modelled using four noded plane stress element (CPS4R). The part bed is modelled as a rigid surface. With a reference node, the rigid surface is modeled as planar rigid surface elements, by IRS21 element. The reference node is specified to define the motion of the rigid body.

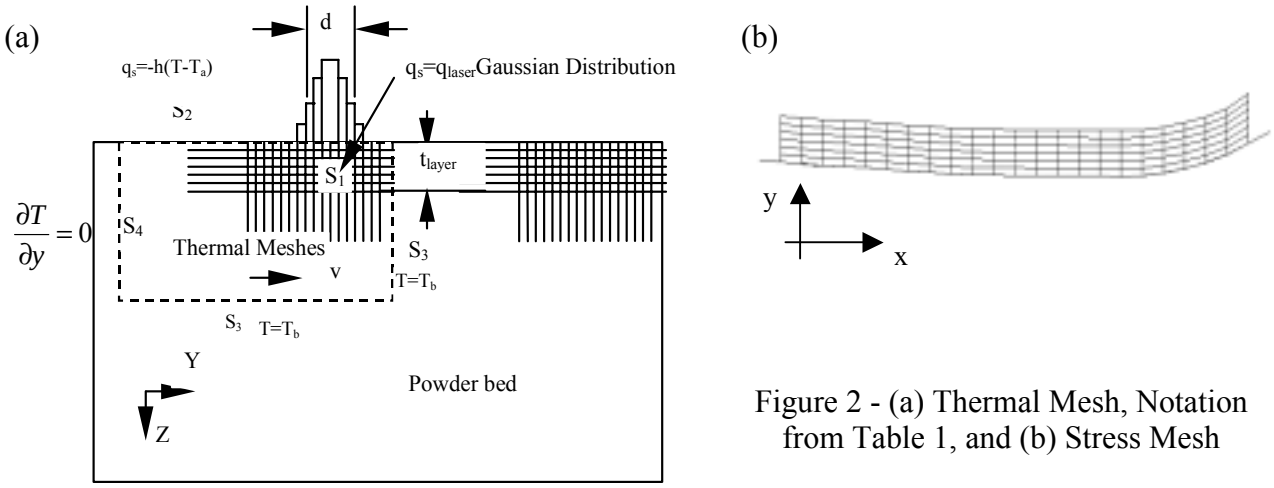

Figure 2 - (a) Thermal Mesh, Notation from Table 1, and (b) Stress Mesh

C specific heat of the material (J/kg K)	v laser blade scan speed (mm/s)
d laser spot diameter (mm)	V unit volume in the material
dh_i thickness of powder layer i after sintering (variable) (mm)	Δh_i thickness of powder layer i before sintering (variable) (mm)
h heat transfer coefficient	ε and ε_{powder} are porosity of sintered part and powder bed respectively
k thermal conductivity of the material (variable) (W/m K)	ρ density of the material (variable) (kg/m^3)
k_s thermal conductivity of solid material (W/m K)	ρ_{powder} density of powder bed (kg/m^3)
l_y,l_z direction cosines of the outward normal to the surface	X solid function
q laser heat flux (W/mm^2)	[C] capacitance matrix,
t_{layer} powder layer thickness (mm)	[K] conductance matrix
T_a ambient temperature (ºC)	{F} heat flux vector
T_b powder bed preheating temperature (ºC)	$\{T\}_{t+\Delta t}$ and $\{T\}_t$ are nodal temperature vectors at time t+Δt and t respectively and Δt is the time step.

Table 1 - Notation

2.3 Material Properties

Material properties, such as the specific heat C, and the thermal conductivity $k_{s,}$, along with elastic modulus E and coefficient of thermal expansion α of solid 316 stainless steel are temperature-dependent, as shown in Fig. 3(a) [11]. In contrast to the heat conduction problem of a solid materials, the thermal conductivity, k, is also a function of temperature and local bed porosity ε, as shown in Fig. 3(b) [9]. The material is modeled as having liquidus temperature of 1380°C, a solidus temperature of 1280°C, and a latent heat of fusion of 308 kJ/kg. The heat transfer coefficient, h, was 5.3 W/m^2K. The powder bed temperature, T_b, is 20°C.

The adopted idealization of the behavior of stainless steel under direct metal SLS process is assumed elastic for temperatures below melting point. The Poisson's ratio is assumed temperature-independent and equal to 0.3.

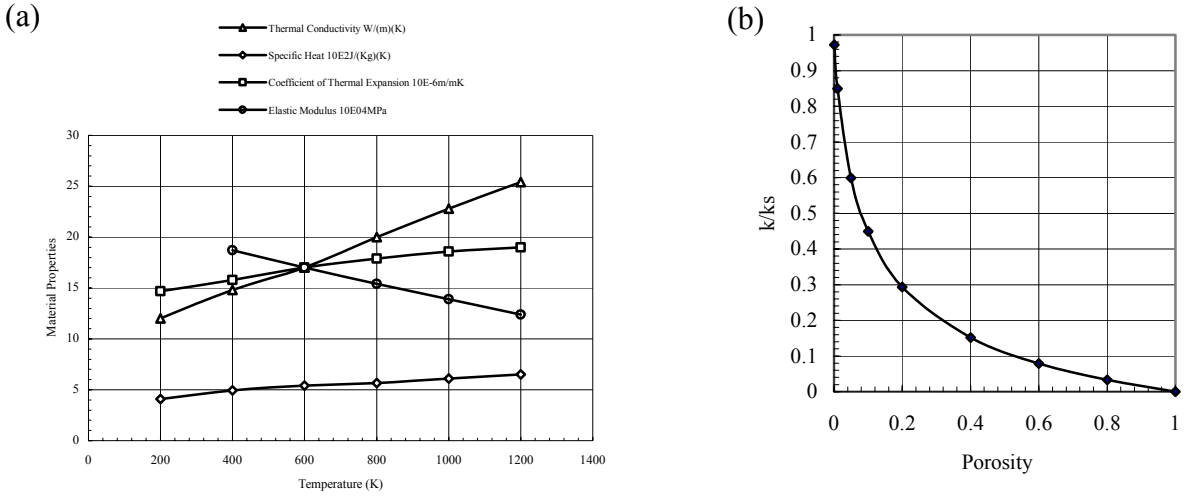

Figure 3 - (a) Temperature Dependence of 316 Stainless Steel properties, and (b) Relationship Between Conductivity and Porosity

2.4 Boundary Conditions and Loading

The boundary conditions for the thermal model can be found in Fig. 2(a).

In mechanical model, the part bed in the analysis is assumed as a rigid surface. The interaction between the part bed and the powder was modeled with a coefficient of friction 0. Although in practice the surface is unlikely to be rigid, it is still assumed to be relatively stiff to the part, and to remain at the same temperature through out the analysis.

A gravity load is applied to all the elements active in the model as a body force. The stress analysis model use the temperature profiles obtained in the heat transfer analysis to define the

thermal loading. Since any change of temperature above the melting point will not produce any stresses, all the temperature beyond the melting point are filtered out by another interface program before it is imported into the mechanical model.

3. RESULTS AND DISCUSSION

3.1 Temperature Profile

Fig. 4(a) shows the transient temperature history as the laser beam moves. The severe temperature gradient during the heating and the significant values of temperatures reached in the course of the analysis can clearly be noted.

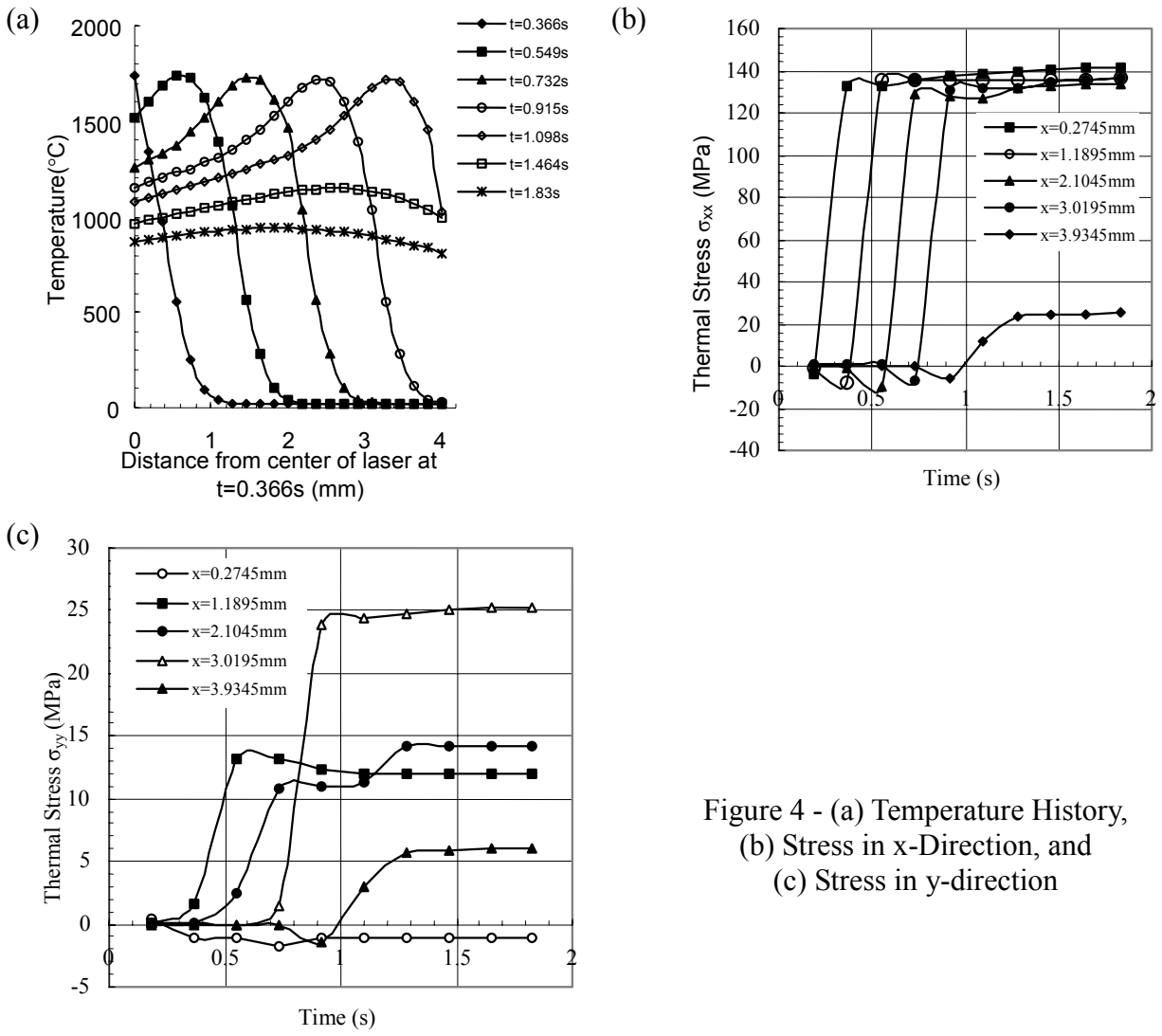

Figure 4 - (a) Temperature History,
(b) Stress in x-Direction, and
(c) Stress in y-direction

3.2 Residual Stresses

Fig. 4(b) shows the thermal stress history within the 0.0833 mm depth of material on the top of the sintered part. For σ_{xx} at all points the part first experiences a slight compression stress, then, as the beam arrives at this point, the metal melts. After the laser beam has past by, cooling occurs, and tensile stresses are generated. The tensile stress becomes greater as the melted metal's strength recovers. Fig. 4(c) shows the correspond thermal stresses σ_{yy} changing with time.

3.3 Deformation

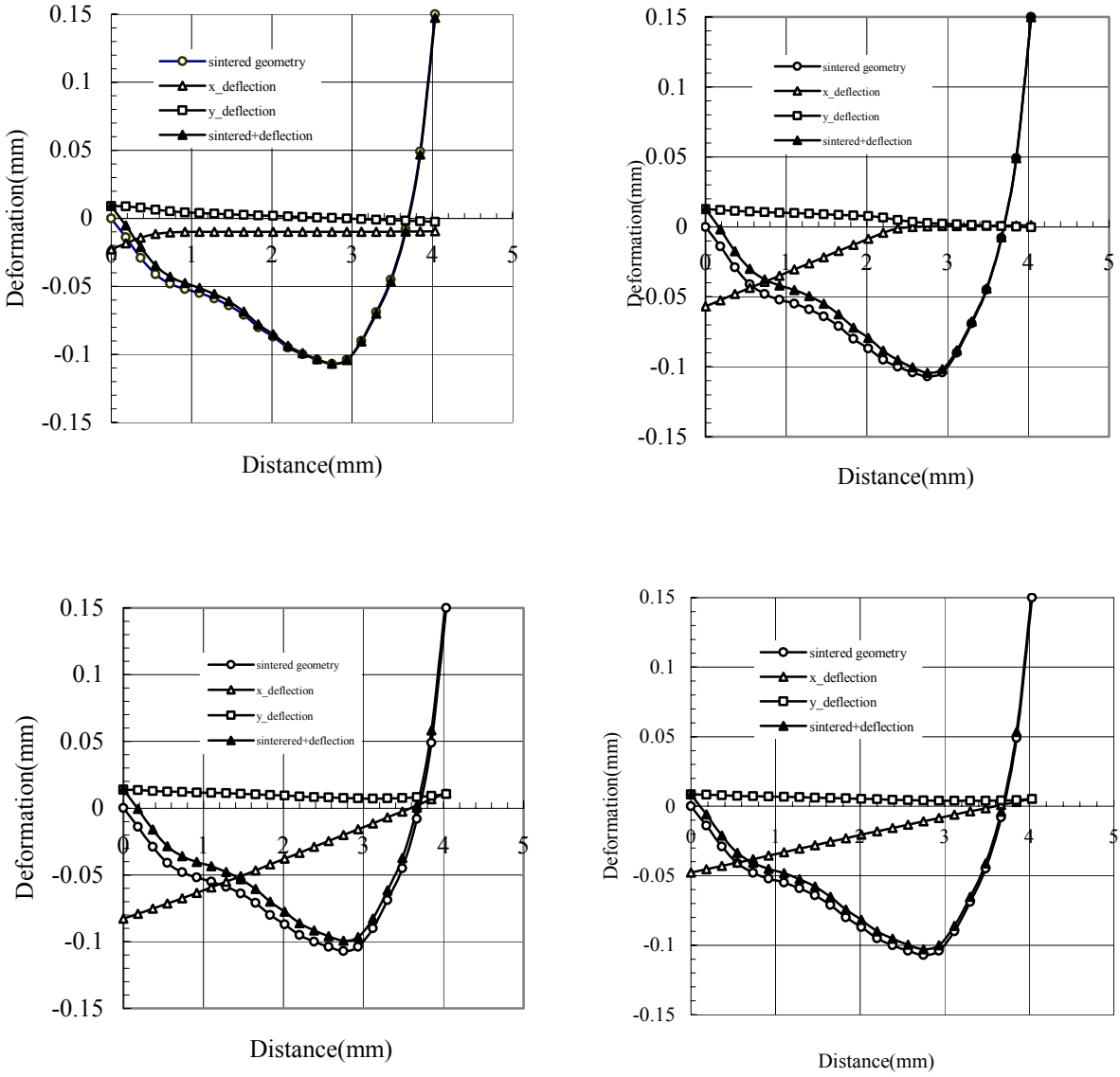

Figure 5 - Developed Deformation Profiles after (a) 0.336 s,
(b) 0.732 s, (c) 1.098 s, and (d) 2.563 s.

There are two mechanisms for deformation development within selectively laser sintered

parts. The first is shrinkage as the result of the sintering process, the second is the result of the thermal stress-induced deflection. These deformation will cause parts warping (curvature) and loss of edge tolerance. Fig. 5 shows the development of these deformations.

The sintered geometry is the coordinates imported from thermal model after filtering out partially sintered region. Thermal loading in the mechanical model will cause deflections in x and y directions. The total deformation in vertical direction is the sum of shrinkage due to solidification and y deflection due to thermal loading. Compared with thermal y deflection, the sintering shrinkage is the main reason for vertical warping and edge tolerance. As the heat source moves along x direction, the thermal deflections in y direction do not change significantly, while in x direction, the thermal deflections increase. After cooling down i.e. at time 2.562s, the x deflection becomes smaller.

4 SUMMARY AND CONCLUSIONS

This research employs finite element method to evaluate the residual stresses and deformations in direct metal SLS process. Three elements of analysis have been involved:

- Modeling the heat transfer problem using a FORTRAN finite element program, with consideration of latent heat and temperature dependent material properties.
- Using interface programs to obtain temperatures below the melting point and the geometry of the fully sintered region, then using them as input to the mechanical model
- Modeling stresses and deformations as a function of time and location for direct metal SLS process using a commercial f.e. code.

From the simulation results we can conclude:

- Excluding edge effects, every position experiences a similar temperature history.
- The deformation in the vertical direction is mainly caused by shrinkage due to the sintering of porous powders, while the deformation in horizontal direction is mainly the result of thermal loading.

ACKNOWLEDGEMENT

WEI JIANG gratefully acknowledge financial support from the China Scholarship Council under Grants 99821129 and National Science Foundation of China under Grants 59935110.

REFERENCES

1. JJ Beaman, JW Barlow, DL Bourell, RH Crawford, HL Marcus, KP McAlea. Solid freeform fabrication: a new direction in manufacturing; Dordrecht London: Kluwer Academic

Publishers, 1997.
2. PF Jacobs, Stereolithography and other RP&M technologies: from rapid prototyping to rapid tooling: Society of Manufacturing Engineers in cooperation with the Rapid Prototyping Association of SME New York: ASME Press, 1996.
3. JC Nelson, S Xue, JW Barlow, JJ Beaman, HL Marcus, DL Bourell. Model of the Selective laser sintering of Bisphenol-A Polycarbonate, Ind. Eng Chem. Res. 1993. 32
4. EM Weissman, & MB Hsu, A Finite Element Model of Multi-layer Laser Sintered part, in Solid Freeform Fabrication Symposium 1991, pp 86-93.
5. M-SM Sun, & JJ Beaman, A three dimensional model for selective laser sintering, in Solid Freeform Fabrication Symposium 1991, pp 102-109.
6. THC Childs, M Berzins, GR Ryder, & AE Tontowi, Selective laser sintering of an amorphous polymer-simulations and experiments, Proc. IMechE Part B, Vol. 213, pp 333-349, 1999.
7. KW Dalgarno, THC Childs, I Rowntree, & L Rothwell, Finite Element Analysis of Curl Development in the Selective Laser Sintering Process, in Solid Freeform Fabrication Symposium 1996, pp 559-566.
8. HS Carslaw, & JC Jaeger, Conduction of heat in Solids, 2nd Edition, Oxford University Press, New York, 1959.
9. TC Tszeng, YT Im, & S Kobayashi, Thermal analysis of solidification by the temperature recovery method., Int. J. Mach. Tools Manufact., 1989, Vol. 29, pp 107-120.
10. THC Childs, C Hauser, CM Taylor & AE Tontowi, Simulation and experimental verification of crystalline polymer and direct metal selective laser sintering, in Solid Freeform Fabrication Symposium 2000, pp 100-109.
11. Metals Handbook Volume 3, Properties and selection: stainless steel, tool materials and special-purpose metals, Metals Park, Ohio: American Society for Metals, 1961